ACTA ONCOLOGICA
2020, VOL. 59, NO. 2, 171–179
https://doi.org/10.1080/0284186X.2019.1679879

Taylor & Francis
Taylor & Francis Group

ORIGINAL ARTICLE

A comparison study between single- and dual-energy CT density extraction methods for neurological proton monte carlo treatment planning

B. van der Heyden[a]*, I. P. Almeida[a,b]*, G. Vilches-Freixas[b], C. Van Beveren[a], A. Vaniqui[a], C. Ares[a], K. Terhaag[a], G. P. Fonseca[a], D. B. P. Eekers[a,b] and F. Verhaegen[a]

[a]Department of Radiation Oncology (MAASTRO), GROW – School for Oncology and Developmental Biology, Maastricht University Medical Centre, Maastricht, Netherlands; [b]Maastro Protonentherapie, Maastricht, Netherlands

ABSTRACT

Monte Carlo proton dose calculations requires mass densities calculated from the patient CT image. This work investigates the impact of different single-energy CT (SECT) and dual-energy CT (DECT) to density conversion methods in proton dose distributions for brain tumours.

Material and methods: Head CT scans for four patients were acquired in SECT and DECT acquisition modes. Commercial software was used to reconstruct DirectDensity™ images in Relative Electron Densities (RED, ρ_e) and to obtain DECT-based pseudo-monoenergetic images (PMI). PMI and SECT images were converted to RED using piecewise linear interpolations calibrated on a head-sized phantom, these fits were referred to as "PMI2RED" and "CT2RED". Two DECT-based calibration methods ("Hünemohr-15it" and "Saito-15it") were also investigated. ρ_e images were converted to mass-densities (ρ_m) to investigate ρ_m differences and one representative patient case was used to make a proton treatment plan. Using CT2RED as reference method, dose distribution differences in the target and in five organs-at-risk (OARs) were quantified.

Results: In the phantom study, Saito-15it and Hünemohr-15it produced the lowest ρ_e root-mean-square error (0.7%) and DirectDensity™ the highest error (2.7%). The proton plan evaluated in the Saito-15it and Hünemohr-15it datasets showed the largest relative differences compared to initial CT2RED plan down to −6% of the prescribed dose. Compared to CT2RED, average range differences were calculated: -0.1 ± 0.3 mm for PMI2RED; -0.8 ± 0.4 mm for Hünemohr-15it, and -1.2 ± 0.4 mm for Saito-15it.

Conclusion: Given the wide choice of available conversion methods, studies investigating the density accuracy for proton dose calculations are necessary. However, there is still a gap between performing accuracy studies in reference ρ_e phantoms and applying these methods in human CT images. For this treatment case, the PMI2RED method was equivalent to the conventional CT2RED method in terms of dose distribution, CTV coverage and OAR sparing, whereas Hünemohr-15it and Saito-15it presented the largest differences.

ARTICLE HISTORY
Received 25 April 2019
Accepted 8 October 2019

Introduction

In conventional radiotherapy, single-energy computed tomography (SECT) images are used to perform dose distribution calculations for treatment planning due to their capability of identifying tissue attenuation characteristics. In the treatment planning procedure, sufficient tumour coverage and healthy tissue sparing are desired. The more advanced photon therapies and proton therapy can lead to conformal tumour dose distributions, allowing optimal sparing of organs-at-risk (OARs) [1–3]. With increasing conformity of tumour dose, the accuracy of the dose calculation algorithm and its input from CT imaging becomes more critical. In this study, we will focus on the accuracy of proton dose calculations based on various information extraction methods from CT images.

In a treatment planning system (TPS) for proton radiotherapy the dose calculation engine requests material properties from the patient CT scan, such as stopping power ratios (SPR) or mass densities (ρ_m), depending on the type of dose calculation algorithm. Most proton centres today base their treatment plan on SECT images, although it has been suggested in the literature that dual-energy CT (DECT) can lead to more accurate proton range prediction [4–8]. In proton radiotherapy, various methods are available to convert SECT and DECT images into ρ_e, which can be converted into ρ_m following a simple linear relationship [9].

In radiotherapy clinics, the CT number to density conversion curve is one of the most commonly used methods [10]. This conversion curve is derived from tissue mimicking phantom measurements with known material properties [11,12]. Alternatively, those tissue mimicking phantom measurement can also be used for the stoichiometric calibration [13] that aims to model CT scanner aspects such as the X-ray spectrum and the detector energy response, and subsequently use this model to predict CT numbers. However, recent studies have shown that stoichiometric methods depend on the tissue mimicking materials used for calibration [14] and

CONTACT F. Verhaegen frank.verhaegen@maastro.nl MAASTRO, Dr Tanslaan 12, 6229 ET Maastricht, The Netherlands
Supplemental data for this article can be accessed here.
*These authors equally contributed to this work.

concluded that the phantom tissue substitutes used in this work seem to be a good representative of biological tissues and that the "stoichiometric calibration becomes unnecessary and may be replaced by a much simpler SECT calibration procedure [14]". Hudobivnik *et al.* [5] investigated the accuracy of the stoichiometric calibration and the CT to density conversion curve for proton stopping power ratios calculated using tissue mimicking inserts similar to the insert materials used in this study. They found mean square error differences compared to the ground truth of 1.8% compared to 1.9% respectively. The CT number to density conversion curve and the stoichiometric calibration are both influenced by the X-ray tube potential, so commercial solutions have been developed to provide an energy independent reconstruction algorithm that directly reconstructs CT numbers into relative electron density (ρ_e, *RED*) units independent from the X-ray tube potential [15].

DECT-based ρ_e conversion methods are less used in clinical routine because radiotherapy treatment planning system do not provide standardised methods for reading DECT images for dose calculations. In 2016, Wohlfahrt *et al.* [7] discussed the clinical implementation of DECT for proton treatment planning based on pseudo-monoenergetic images (PMIs).

In this study, the ρ_e accuracy of two SECT and three DECT-based ρ_e conversion methods were evaluated in a phantom study with accurately known material properties. Additionally, these five conversion methods were studied in four patient brain CT scans. A proton treatment plan was created for one patient and differences in dose distribution, particularly target coverage and sparing of OARs, were quantified.

Material and methods

Phantom study and CT protocols

Two ρ_e phantoms with certified chemical compositions and densities were scanned with a SOMATOM Confidence® RT pro 64-slice CT scanner (Siemens Healthineers, Forchheim, Germany) in SECT acquisition mode at 120 kVp and dual-spiral DECT acquisition mode at 80 and 140 kVp. All phantom scans were reconstructed with sinogram affirmed iterative reconstruction (SAFIRE, Siemens terminology) with beam hardening correction for bone enabled (Q34 kernel, strength 3). The SECT scan was also reconstructed with the commercially available iterative DirectDensity™ (Siemens Healthineers) reconstruction algorithm (F30 kernel, strength 3) (15). DirectDensity™ is a projection-based algorithm that reconstructs SECT scans in RED image intensities independently from the X-ray tube potential and without additional user calibrations. For all phantom acquisitions, the X-ray tube current (mAs) was manually set to have a constant CT dose index (32 cm) of approximately 30 mGy. Compared to the clinical scanning protocols, a higher CT dose index was chosen to limit noise influences in the phantom study. Instead of a 16 cm CT dose index, the 32 cm dose index was reported for this phantom study because the shoulders were also imaged according to our clinical neurological scan protocol. In the manufacturer's neurological scan protocol (16 cm), the patient's shoulders also exceed the limited field-of-view.

The first phantom was a head-size home-made PMMA cylinder (diameter = 15.0 cm, length = 28.0 cm) consisting of one central hole (diameter = 2.8 cm) drilled through the entire cylinder length to fit four RMI 467 tissue characterisation inserts (Gammex Inc., Middleton, WI) simultaneously. Different insert combinations were inserted in the PMMA phantom so that a total of 14 tissue mimicking inserts were scanned. The second phantom was the central bulk and the inserts of the 062 M phantom (CIRS Inc., Norfolk, VA). The mean CT_{HU} numbers of each insert from both phantoms were computed in a cylindrical volume-of-interest containing seven central axial CT slices and two-dimensionally eroded with four pixels in the axial CT planes to avoid the insert edges. Symbol CT_{HU} is used to denote CT numbers in Hounsfield Units (HU). The PMMA phantom was used for the calibration of four ρ_e conversion methods, and the validation of DirectDensity™, whereas the 062 M phantom was used for the validation of all five conversion methods.

ρ_e conversion methods

Single-energy CT

This paper examines two SECT methods to convert CT_{HU} numbers to ρ_e. In the first conversion method, the cylindrical PMMA phantom was used to obtain the energy dependent CT_{HU} number to ρ_e conversion curve for the 120 kVp acquisition (called "CT2RED" onwards). The CT to ρ_e conversion curve was then applied to the 062 M validation phantom.

In the second conversion method, the 120 kVp acquisition of both phantoms was reconstructed by DirectDensity™, which should be independent of the X-ray tube potential and reconstructs directly into CT_{RED} numbers [15]. CT_{RED} denotes CT numbers in units that are linearly scalable to ρ_e using a fixed linear relationship: $\rho_e = CT_{RED}/1000 + 1$ [15]. No additional ρ_e calibration procedure was required and therefore, the ρ_e values of both phantoms were used for validation of this method.

Dual-energy CT

This paper examines three DECT based CT_{HU} number to ρ_e conversion methods. In the first method, Saito's methodology [16] was used to convert the DECT images into ρ_e. This method uses a linear fit procedure between a weighted subtraction of the 80 and 140 kVp CT images to obtain scanner and protocol specific fit parameters *a*, *b* and α

$$\rho_e = a \cdot \frac{(1+\alpha)CT^H_{HU} - \alpha\ CT^L_{HU}}{1000} + b \qquad (1)$$

The mean 80 and 140 kVp CT_{HU} numbers of the PMMA phantom inserts (CT^L_{HU} and CT^H_{HU}) computed in cylindrical regions-of-interest in the middle of the inserts, were used in the calibration procedure. As validation, the CT^L_{HU} and CT^H_{HU} of the 062 M validation phantom were combined according to Equation 1. Furthermore, a denoising algorithm was applied in the resulting ρ_e images, which consisted of an edge-preserving curvature flow image filter (time step = 0.05, iterations = 15) implemented in the Insight

Segmentation and Registration Toolkit (ITK) [17]. This implementation is denoted as "Saito-15it".

In the second DECT based extraction method ("Hünemohr-15it"), Hünemohr's methodology [6] was used to calculate the ρ_e image. This methodology starts from the same equation as Saito's method [18–20], performing a weighted subtraction of the 80 and 140 kVp CT images, but bases its calibration on one single fit parameter (c_e) according to Equation 2. This method is implemented in *syngo*.via's RHO/Z package (Siemens Healthineers, VB30) and is therefore added to this study. Currently, the *syngo*.via VB30 software uses a non-system specific and default fit parameter (c_e) to calculate the ρ_e images. Our Hünemohr-15it implementation, which is based on a dedicated calibration fit, derived this c_e fit parameter for a body site specific and system specific protocol (SOMATOM Confidence RT Pro) and serves as the best-case scenario possible to achieve with *syngo*.via as commercial software. The effect of denoising was investigated in Supplementary Material A.

$$\rho_e = c_e \cdot \left(\frac{CT^H_{HU}}{1000} + 1\right) + (1 - c_e)\left(\frac{CT^L_{HU}}{1000} + 1\right) \quad (2)$$

The third and last DECT based ρ_e extraction method used a pseudo monoenergetic CT_{HU} number to ρ_e conversion curve. Here the PMI was calculated by *syngo*.via's Monoenergetic Plus algorithm; this method will be denoted "PMI2RED" onwards [21]. Following Wohlfahrt *et al.* [7], the PMI was reconstructed at 79 keV. The same calibration procedure was used to obtain the CT2RED and PMI2RED conversion curves. Both conversion curves are added as Supplementary Material B and the schematic study workflow is depicted in Supplementary Material C.

Brain tumour CT scans

A mass density comparison was performed for all patients and one patient dataset was used to perform proton dose calculations on the mass density datasets (Supplementary Material C).

CT protocol and post-processing

To evaluate ρ_m differences between the different ρ_e conversion methods, brain CT scans of four patients were acquired with a contrast-enhanced SECT imaging protocol and a dual-spiral 80 and 140 kVp DECT imaging protocol using the SOMATOM Confidence® RT pro CT scanner. After the contrast medium injection (iodine), a latency time of 5 min was considered before starting the SECT scan, after that the DECT scan was directly acquired (<1 min). The impact of the contrast medium on the images was investigated for one of the patients (Supplementary Material D). All scans were acquired with a constant CT dose index (32 cm) of 20 mGy and reconstructed with a voxel dimension of $0.64 \times 0.64 \times 1.00\,mm^3$. The study was approved by the internal review board of Maastro Clinic (P0243).

The SECT and DECT acquisitions were reconstructed with the SAFIRE technique with beam hardening correction for bone enabled (Q34 kernel, strength 3). Additionally, the SECT-based DirectDensity™ reconstruction (F30 kernel, strength 3) was performed for one representative patient, since this algorithm is not recommended for proton therapy[1]. The DECT reconstructions were registered using deformable image registration software (Elastix) [22], and post-processed to calculate the ρ_e images based on Saito's and Hünemohr's methods. Additionally, *syngo*.via's DECT software package was used to calculate the PMIs at 79 keV.

A proton treatment plan was created for one of the four brain CT scan with a fictitious tumour and prior to the planning stage, the five ρ_e images were converted to ρ_m by using a linear fit relationship (maximum fit error <1%) based on human tissues and recommended in TG186 [9]: $\rho_m = -0.175 + 1.176 \cdot \rho_e$ $(R^2 = 0.99992)$. Between the CT acquisitions, the anatomy of the patient can change due to motion, therefore all ρ_m images originating from the DECT conversion methods were elastically deformed to the ρ_m image originating from the SECT 120 kVp scan. Finally, the same values of ρ_m for the voxels outside the body structure were assigned in all sets to assure that the differences found in the treatment plan were caused only by the ρ_m values of the patient geometry.

Proton treatment planning

The Clinical Target Volume (CTV) corresponding to a fictitious brain tumour (craniopharyngioma), as well as the OARs were delineated by a radiation oncologist in the conventional 120 kVp SECT scan. A pencil beam scanning treatment plan was made in RayStation v8A Monte Carlo (RaySearch Laboratories AB, Stockholm, Sweden) using the CT2RED ρ_m-image. Three coplanar fields (one posterior and two lateral) were aimed at the CTV with a prescription dose of 54 Gy (RBE) in 30 fractions (Figure 1). The beam angles (80°, 180°, 290°) were chosen to avoid crossing the right and left hippocampi, which have a low dose tolerance ($D_{40\%} \leq 7.3$ Gy) [23]. The optical chiasm with a tolerance of $D_{0.03\,cc} \leq 55$ Gy is located at the distal edge of the posterior beam [23].

The optimisation toolbox and the RayStation Monte Carlo dose engine were used to compute the final dose with 0.5% statistical uncertainty in the CT2RED ρ_m image. After this, the final plan was recalculated, without performing a new optimisation, in the other four sets of density images (DirectDensity™, PMI2RED, Hünemohr-15it and Saito-15it) and relative differences between the CT2RED and the other dose distributions were assessed. Furthermore, dose volume histograms (DVH) for the CTV and selected OARs (optical chiasm, brainstem, hippocampi and pituitary gland) were analysed. Finally, a plan with a single posterior beam (beam 3 in Figure 1) was made with the purpose of quantifying differences in proton range (defined as the 80% distal fall-off) between the different methods. Beam 3 was chosen to investigate the dose influence on the chiasm.

Results

Calculated relative electron density accuracy in phantoms

The relative difference between the determined ρ_e by the five conversion methods and the certified ρ_e for the PMMA

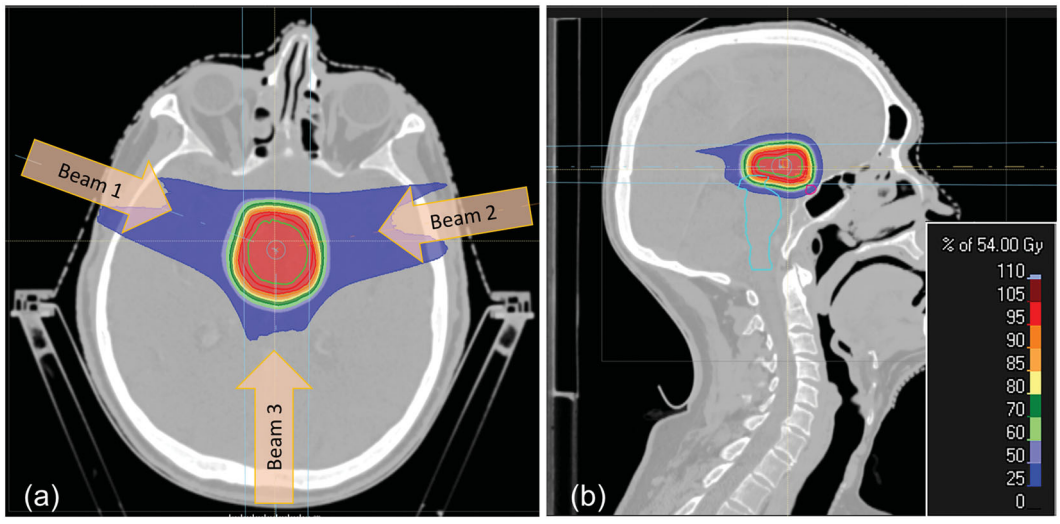

Figure 1. A proton treatment plan with a fictitious brain tumour irradiated by three proton beams was created to evaluate dose and proton range differences for one example patient.

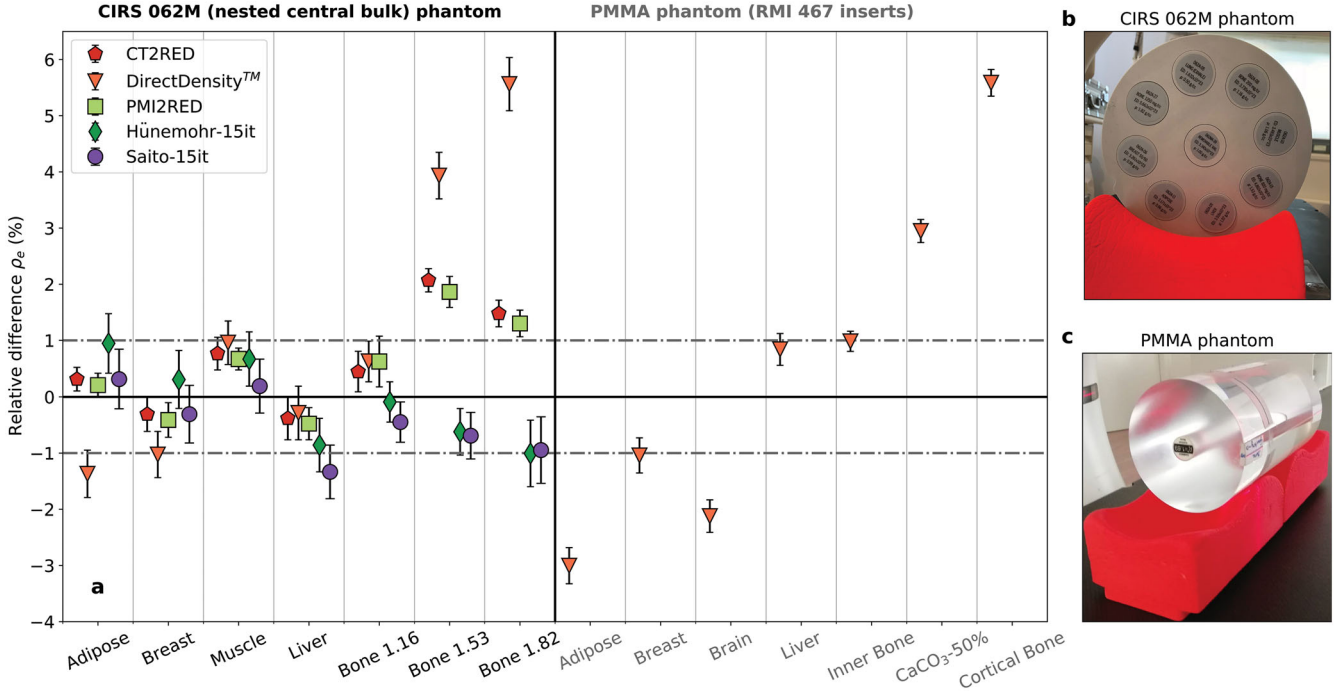

Figure 2. The relative ρ_e difference (%) (measurement-reference) for the five conversion methods. The error bars indicate ± 1 standard deviation (a) On the left, the differences were calculated for the 062 M phantom. On the right, the differences were calculated for the PMMA phantom. The measurement setup is illustrated in (b) and (c).

and 062 M phantoms is illustrated in Figure 2(a). In both phantoms, the largest ρ_e errors were found in the high-density bone inserts for the DirectDensity™ image reconstruction method. Compared to the manufacturer's ρ_e certificate, DirectDensity™ overestimated the ρ_e of 'Bone 1.53' by 3.9% and 'Bone 1.82' by 5.5%. The lowest root-mean-square (RMS) errors for ρ_e were found for the Saito-15it ($a = 0.999$, $b = 0.995$, $\alpha = 0.864$) and the Hünemohr-15it ($c_e = 0.873$) methods, which were below ±1.0%. Overall, the RMS errors for the 062 M inserts were 2.7% for DirectDensity™ and 1.0% for CT2RED and PMI2RED.

The standard deviations calculated in the inserts for the Saito-15it and the Hunemohr-15it methods were larger compared to the other conversion methods, although edge-preserving denoising was applied as post-processing (Supplementary Material A). Between these two DECT methods, no significant differences in RED calculation were observed. ($p = .003$, paired t-test). The CT2RED and PMI2RED methods showed comparable errors; only in the medium and high-density bone inserts, the ρ_e errors were larger than 1.4% for both methods.

Mass density differences in the patient geometries

Absolute ρ_m differences (g/cm^3) in arbitrary cranial slices between the conventional CT2RED conversion method and

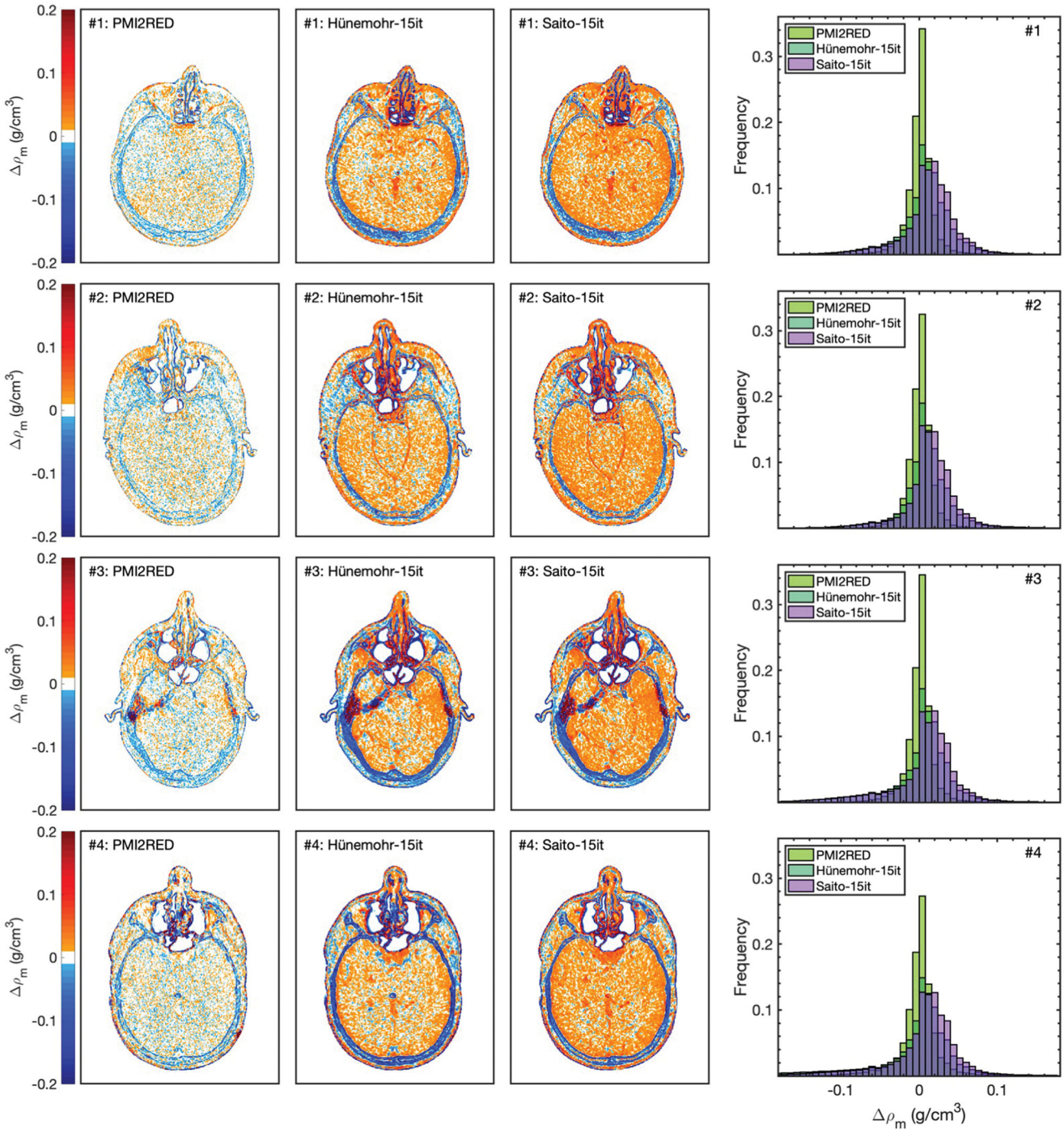

Figure 3. Absolute mass density differences ($\Delta\rho_m$) are shown in one representative CT slice for each of the four patients (#1-4). Differences are calculated for the PMI2RED, Hünemohr-15it and Saito-15it conversion methods minus the conventional reference CT2RED. In the right panels, the frequency histogram is shown over the entire CT image excluding air cavities and dental artefacts.

three other methods are depicted in Figure 3 for the different brain CT scans. In the right column of Figure 3, a histogram indicates the normalised frequency distribution of the absolute ρ_m differences in bins of 0.01 g/cm^3 between the conventional CT2RED method (as reference) and the PMI2RED, Hünemohr-15it and Saito-15it conversion methods. For each of the four brain CT scans, Figure 4 shows the average ρ_m differences for all tissues (excl. air cavities and dental filling artefacts), but also for the soft tissues ($0.9 < \rho_m < 1.2$ g/cm^3) and for bone tissues ($\rho_m \geq 1.2$ g/cm^3) separately. Air cavities were excluded by thresholding ($\rho_m < 0.2$ g/cm^3) and dental artefacts were excluded by manual artefact segmentation. The DirectDensity™ results for patient #1 are shown in Supplementary Material E.

With respect to CT2RED, the PMI2RED (-0.01 ± 0.01 g/cm^3), Hünemohr-15it (-0.04 ± 0.04 g/cm^3) and Saito-15it (-0.02 ± 0.02 g/cm^3) conversion methods resulted in overall lower bone densities (i.e., negative differences compared to CT2RED) averaged over the four brain CT scans. For the same conversion methods, overall positive differences were observed for the soft tissues: 0.003 ± 0.001 g/cm^3, 0.011 ± 0.002 g/cm^3 and 0.018 ± 0.001 g/cm^3, respectively.

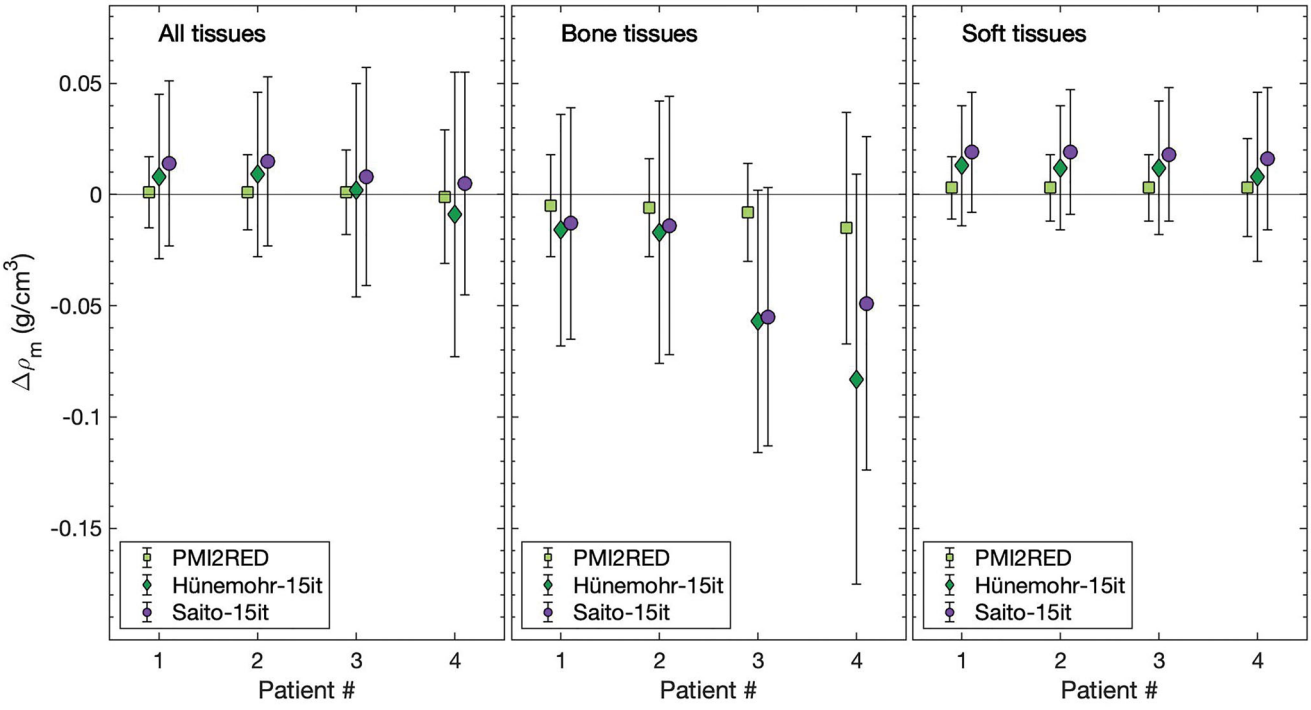

Figure 4. Mass density differences ($\Delta\rho_m$) (± 1 standard deviation) for the PMI2RED, Hünemohr-15it and Saito-15it methods minus the conventional CT2RED conversion method calculated over the entire patient geometry excluding air and dental fillings, for all tissues (left), only for bone tissues (middle) and only for soft tissues (right panel).

Differences in proton dose distributions

Relative dose differences between the CT2RED and the other three conversion methods for a representative axial CT image slice of the transversal plane are shown in Figure 5(a–c). The plan evaluated on the Saito-15it image shows the largest differences compared to the initial plan (down to −6%), followed by the Hunemohr-15it method (down to −4%) and the PMI2RED method (almost no visible differences). The DVHs resulting from each plan are depicted in Figure 5(d) for the CTV and five selected OARs, with the DVH of the CTV zoomed-in on Figure 5(e).

For the dose from one posterior beam, differences in proton range resulted in an average of -0.1 ± 0.3 mm for PMI2RED; -0.8 ± 0.4 mm for Hünemohr-15it, and -1.2 ± 0.4 mm for Saito-15it.

Discussion

The recent availability of CT scanners with DECT capabilities in addition to the standard SECT mode, and different methods of converting CT_{HU} or CT_{RED} numbers to ρ_e in radiotherapy facilities raises the question which one to use and its impact on treatment planning. This study aims to investigate the differences in relative electron densities and dose calculations for proton treatment planning depending on which conversion method is used: CT2RED, PMI2RED, Hünemohr-15it and Saito-15it, from which the first two methods are part of commercially available software.

Initially, the ρ_e accuracy was assessed in two phantoms. The 062 M phantom was used as validation phantom for all methods and relative errors with respect to the reference ρ_e showed a higher discrepancy in the high-density materials (Figure 1). Saito-15it and Hunemohr-15it had the lowest root-mean-square (RMS) error of 0.7%, whereas DirectDensity™ showed the highest RMS error of 2.7%. This study used head-sized phantoms, but it should be noted that the DirectDensity™ algorithm does not support user calibration and is developed by Siemens Healthineers on an abdominal-sized phantom[2]. It is expected that the RED accuracy of the DirectDensity™ will improve when the algorithm is optimised for head-sized volumes, however this remains speculation and needs further investigation.

With SECT and DECT scans from four patients, ρ_e images were created using each conversion method and converted in ρ_m using the recommendation from TG186 [9]. Lacking a ground truth for the patient scans, the CT2RED ρ_m images were used as reference because this method is used at our institute for photon (Eclipse TPS, Varian Medical Systems) and for proton dose calculations. Differences with the other conversion methods were assessed (Figures 3 and 4).

The Hünemohr-15it method aims to reproduce the results that the commercial *syngo*.via RHO/Z package would give, if a proper scanner-, size- and energy-specific calibration were used. Scanner and body site specific calibration parameters could not be adapted in the *syngo*.via version installed at our institution, therefore our own implementation of the method had to be used. The use of this commercial RHO/Z package without an optimal calibration might result in relative electron density discrepancies and dose distribution differences. The ability to specify scan-specific fit parameters in clinical software would be beneficial for the accuracy of the relative electron density images and furthermore the radiotherapy dose calculations.

The dose distribution discrepancies caused by the ρ_m differences were investigated for one example patient, in which the

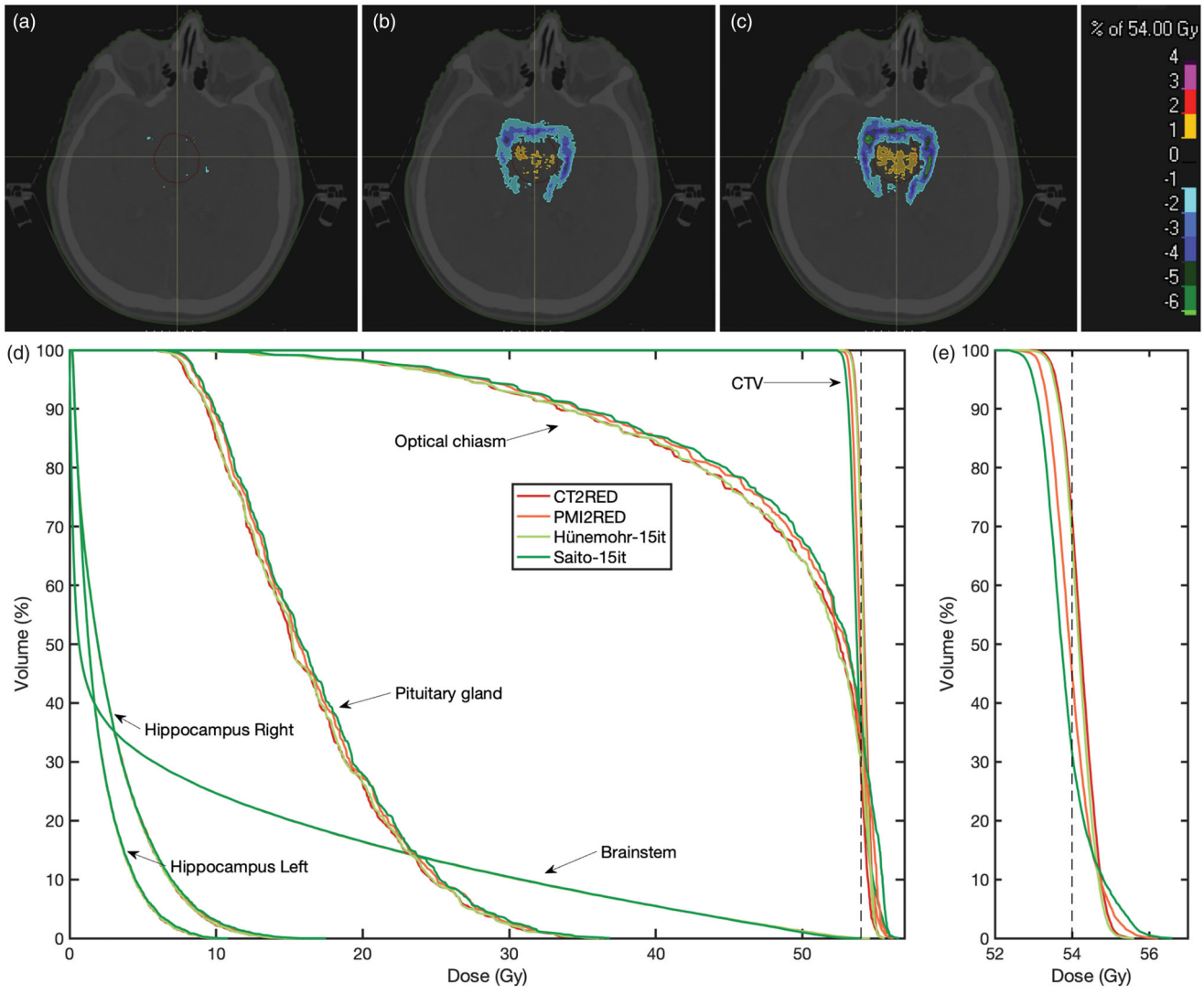

Figure 5. Top panel: dose differences between the plan calculated on the CT2RED images and the same plan evaluated on (a) PMI2RED, (b) Hünemohr-15it and (c) Saito-15it datasets. Bottom panel: (d) dose volume histograms of the five evaluated methods for the CTV (solid line) and five organs-at-risk; (e) zoomed-in CTV dose volume histogram. The method specific DVH curves for the brainstem largely overlap.

CT2RED derived dataset was used as reference. In the planning stage of this treatment plan, robust planning [24] was considered to follow the trend in clinical practice to account for set-up and range uncertainties, but it was found that a robust plan did not alter the main conclusions shown. Therefore, no robust optimisation was used in this study. Results in Figure 5(a–c) agree with the ρ_m differences observed in Figures 3 and 4. The contributions of bone and soft tissues to these dose differences were assessed and it was found that, although dense bone tissues show the higher absolute ρ_m differences between methods, it has a negligible contribution for this patient plan because the proton beam path through brain tissue is much longer than the beam path through bone.

For the single posterior beam plan (beam 3), average 80% distal fall-off range differences were reported between −1.2 mm (Saito-15it) and 0.1 mm (PMI2RED) which fall within the voxel size of $(1\,\text{mm})^3$ typically used in radiotherapy for head CT scans. The 0.1 ± 0.3 mm difference found with the PMI2RED conversion is lower but comparable to the 0.3 mm range reported for a head-and-neck cancer patient by Wohlfahrt *et al.* [7] where the hypothetical treatment beam had to pass more bone than in our treatment plan.

The optical chiasm and pituitary gland show the largest differences in DVH for the three methods, because of their location in the distal edge of the posterior beam and their small volume, making them more sensitive to small variations. In contrast, the brainstem and hippocampi show similar dose coverages for all methods, since these organs are not in the beam paths. To follow up on this study, a larger cohort of patients and different sites should be analysed to confirm the robustness and consistency of each method.

Given the wide choice of commercially available methods for converting SECT and DECT images to ρ_e, studies are needed to assess the accuracy of these methods, as well as its impact for proton dose calculations. However, there is still a gap between performing accuracy studies in certified ρ_e phantoms with known compositions and applying these methods in human CT images. Furthermore, full-DECT treatment planning is currently not an option in commercial TPS, where the only solution for the user is to pre-process the DECT images and use the resulting

ρ_m (or SPR) image as input [25]. This work quantifies the differences in ρ_m for four patients and quantifies differences in dose and proton range for a neurological patient between the conventional CT2RED method and three other SECT- or DECT- based conversion methods. For this treatment site, the PMI2RED method was equivalent to the conventional CT2RED method in terms of dose distribution, CTV coverage and dose to the OARs, whereas Hünemohr-15it and Saito-15it led to differences in proton dose and range. Which method approximates best reality in a patient cannot be determined in this study. However, the mass density differences observed in our patient cohort were in agreement with the differences observed in the phantom study. In this phantom study, DECT-based methods with body site and protocol specific calibration such as Hünemohr-15it and Saito-15it achieved the highest relative electron density accuracy, which allows to speculate that these methods also achieved the highest accuracy in our patient cohort. Furthermore, the dose differences between the different conversions were in agreement with previously published research [4,26].

Not only further research is required to evaluate the accuracy of the available conversion methods in larger patient cohorts or in realistic phantom geometries with known material properties, also efforts from the imaging and TPS manufacturers are required to improve the accuracy of the radiotherapy dose calculations. Clinics should be enabled to set optimised DECT parameters (e.g., c_e fit coefficient in Hünemohr-15it) according to their clinical scan protocols and should be enabled to directly use post-processed DECT acquisitions in the TPS to perform dose calculations.

Notes

1. Private correspondence with Siemens Healthineers.
2. Private correspondence with Siemens Healthineers.

Acknowledgements

The authors thank Prof. Dr. Katia Parodi, head of the Department of Medical Physics, Faculty of Physics, Ludwig-Maximilians-Universität München (LMU), for lending the PMMA head size phantom. Dr. Christian Hofmann and Dr. Jens-Christoph Georgi from Siemens Healthineers and Dr. Guillaume Landry from LMU are acknowledged for their valuable comments and discussion on this work.

Disclosure statement

The authors report no conflicts of interest. The authors alone are responsible for the content and writing of the paper.

References

[1] Jakobi A, Bandurska-Luque A, Stutzer K, et al. Identification of patient benefit from proton therapy for advanced head and neck cancer patients based on individual and subgroup normal tissue complication probability analysis. Int J Radiat Oncol Biol Phys. 2015;92(5):1165–1174.

[2] van de Water TA, Bijl HP, Schilstra C, et al. The potential benefit of radiotherapy with protons in head and neck cancer with respect to normal tissue sparing: a systematic review of literature. Oncologist. 2011;16(3):366–377.

[3] Weber DC, Wang H, Cozzi L, et al. RapidArc, intensity modulated photon and proton techniques for recurrent prostate cancer in previously irradiated patients: a treatment planning comparison study. Radiat Oncol. 2009;4(1):34.

[4] Almeida IP, Schyns L, Vaniqui A, et al. Monte Carlo proton dose calculations using a radiotherapy specific dual-energy CT scanner for tissue segmentation and range assessment. Phys Med Biol. 2018;63(11):115008.

[5] Hudobivnik N, Schwarz F, Johnson T, et al. Comparison of proton therapy treatment planning for head tumors with a pencil beam algorithm on dual and single energy CT images. Med Phys. 2016;43(1):495.

[6] Hunemohr N, Krauss B, Tremmel C, et al. Experimental verification of ion stopping power prediction from dual energy CT data in tissue surrogates. Phys Med Biol. 2014;59(1):83–96.

[7] Wohlfahrt P, Mohler C, Hietschold V, et al. Clinical implementation of Dual-energy CT for proton treatment planning on Pseudo-monoenergetic CT scans. Int J Radiat Oncol Biol Phys. 2017;97(2):427–434.

[8] Wohlfahrt P, Mohler C, Stutzer K, et al. Dual-energy CT based proton range prediction in head and pelvic tumor patients. Radiother Oncol. 2017;125(3):526–533.

[9] Beaulieu L, Carlsson Tedgren A, Carrier JF, et al. Report of the Task Group 186 on model-based dose calculation methods in brachytherapy beyond the TG-43 formalism: current status and recommendations for clinical implementation. Med Phys. 2012;39(10):6208–6236.

[10] Taasti VT, Michalak GJ, Hansen DC, et al. Validation of proton stopping power ratio estimation based on dual energy CT using fresh tissue samples. Phys Med Biol. 2017;63(1):015012.

[11] Constantinou C, Harrington JC, DeWerd LA. An electron density calibration phantom for CT-based treatment planning computers. Med Phys. 1992;19(2):325–327.

[12] Das IJ, Cheng CW, Cao M, et al. Computed tomography imaging parameters for inhomogeneity correction in radiation treatment planning. J Med Phys. 2016;41(1):3–11.

[13] Schneider U, Pedroni E, Lomax A. The calibration of CT Hounsfield units for radiotherapy treatment planning. Phys Med Biol. 1996;41(1):111–124.

[14] Goma C, Almeida IP, Verhaegen F. Revisiting the single-energy CT calibration for proton therapy treatment planning: a critical look at the stoichiometric method. Phys Med Biol. 2018;63(23):235011.

[15] van der Heyden B, Öllers M, Ritter A, et al. Clinical evaluation of a novel CT image reconstruction algorithm for direct dose calculations. Physics Im Radiat Oncol. 2017;2:11–16.

[16] Saito M. Potential of dual-energy subtraction for converting CT numbers to electron density based on a single linear relationship. Med Phys. 2012;39(4):2021–2030.

[17] Malladi R, Sethian JA. Image processing: flows under min/max curvature and mean curvature. Graph Model Im Proc. 1996;58(2):127–141.

[18] Almeida IP, Landry G, van Elmpt W, et al. Reply to: "Comment on: Dual-energy CT quantitative imaging: a comparison study between twin-beam and dual-source CT scanners [Med Phys. 44(1), 171-179 (2017)]. Med Phys. 2018;45(8):3997–3998.

[19] Almeida IP, Schyns LE, Ollers MC, et al. Dual-energy CT quantitative imaging: a comparison study between twin-beam and dual-source CT scanners. Med Phys. 2017;44(1):171–179.

[20] Saito M. Comment on: Dual-energy CT quantitative imaging: a comparison study between twin-beam and dual-source CT scanners [Med Phys. 44(1), 171–179 (2017)]. Med Phys. 2018;45(8):3996–3996.

[21] Grant KL, Flohr TG, Krauss B, et al. Assessment of an advanced image-based technique to calculate virtual monoenergetic computed tomographic images from a dual-energy examination to improve contrast-to-noise ratio in examinations using iodinated contrast media. Invest Radiol. 2014;49(9):586–592.

[22] Klein S, Staring M, Murphy K, et al. Elastix: a toolbox for intensity-based medical image registration. IEEE Trans Med Imaging. 2010;29(1):196–205.

[23] Lambrecht M, Eekers DBP, Alapetite C, et al. Radiation dose constraints for organs at risk in neuro-oncology; the European Particle Therapy Network consensus. Radiother Oncol. 2018;128(1):26–36.

[24] Unkelbach J, Paganetti H. Robust proton treatment planning: physical and biological optimization. Semin Radiat Oncol. 2018; 28(2):88–96.
[25] Wohlfahrt P, Mohler C, Richter C, et al. Evaluation of Stopping-Power prediction by Dual- and Single-Energy computed tomography in an anthropomorphic Ground-Truth phantom. Int J Radiat Oncol Biol Phys. 2018;100(1):244–253.
[26] Bar E, Lalonde A, Zhang R, et al. Experimental validation of two dual-energy CT methods for proton therapy using heterogeneous tissue samples. Med Phys. 2018;45(1):48–59.